Electromagnetic Design Characterization of a Dual Rotor Axial Flux Motor for Electric Aircraft

Dorsa Talebi
Dept. of Elec. & Comp. Engr.
Texas A&M University
College Station, TX, USA
dorsa.talebi@tamu.edu

Matthew C. Gardner
Dept. of Elec. & Comp. Engr.
University of Texas at Dallas
Richardson, TX, USA
Matthew.Gardner@utdallas.edu

Sri Vignesh Sankarraman
Dept. of Elec. & Comp. Engr.
University of Texas at Dallas
Richardson, TX, USA
SriVignesh.Sankarraman@utdallas.edu

Ahmad Daniar
Dept. of Elec. & Comp. Engr.
University of Texas at Dallas
Richardson, TX, USA
Ahmad.Daniar@utdallas.edu

Hamid A. Toliyat
Dept. of Elec. & Comp. Engr.
Texas A&M University
College Station, TX, USA
toliyat@tamu.edu

***Abstract*— This paper presents and evaluates a dual rotor axial flux permanent magnet motor for electric aircraft applications. Several features, including grain oriented electrical steel, Halbach arrays, and wires with rectangular cross-sections, are used to improve torque density and efficiency. A novel winding arrangement is used to mitigate interturn short-circuit faults. Rather than simply optimizing the motor by itself, this paper evaluates the tradeoffs between motor performance and its interfaces with the drive, thermal management system (TMS), and mechanical structure. This information can be used along with similar analyses of these subsystems to select the design with the system-level optimal performance. The paper uses finite element simulations to characterize tradeoffs between active mass, efficiency, fundamental frequency, power factor, axial forces on the rotors, and cooling surface area. Several designs exceed 95% efficiency at takeoff with less than 8 kg of active mass. While high pole counts, a large outer radius, and short stator teeth tend to optimize the magnetic performance at takeoff, this can reduce cruise efficiency, reduce the surface area through which the TMS can extract heat, increase the fundamental frequency the drive must supply, increase the structural mass required to support the rotors, and introduce complexity to manufacturing process. Further analysis for a selected design reveals that the power factor can be significantly improved with a minimal torque penalty via field weakening, due to significant saturation in the stator teeth.**

Keywords*— *Axial flux PM machine, dual rotor, grain oriented electrical steel, segmented Halbach array, NdFeB magnets, yokeless and segmented armature (YASA), rectangular wire, co-design, slot/pole combination, fractional-slot concentrated windings, finite element analysis, electric aircraft, interturn short-circuit fault

I. Introduction

Pure electric and hybrid electric aviation require the weight of the motor, drive, and associated cooling to be minimized [1], [2]. Thus, the US Advanced Research Projects Agency-Energy (ARPA-E) aviation-class synergistically cooled electric motors with integrated drives (ASCEND) program promotes a highly efficient, ultra-lightweight motor, drive, and thermal management system (TMS) for aircraft propulsion with targets listed in Table I [3]. The 12 kW/kg at 5000 RPM target specific power (including motor, drive, and TMS) must be sustained for a minute and gradually ramped down over 20 minutes, as shown in Fig.1. This represents a significant improvement over the state-of-the-art 5 kW/kg aviation motor built by Siemens [4]. Achieving this target will require aggressive designs with tight integration and co-design of the different subsystems and physics.

For this project, an axial flux permanent magnet (AFPM) motor, which is illustrated in Fig. 2, is proposed with several features to achieve a high torque density and a target of 95% efficiency at the peak power. The yokeless and segmented armature (YASA) topology has demonstrated high performance with high current densities [5], which will be required for takeoff. The use of a segmented armature along with the fractional slot concentrated winding facilitates higher slot fill factors [5], [6]. Moreover, the fractional slot concentrated winding (FSCW) configuration improves phase independence and fault tolerance [5]. The shorter end windings in the YASA topology improve the torque density of the motor [6], [7]. Additionally, this topology reduces core losses by replacing the stator yoke with an additional rotor [5], [8], [9]. Grain-oriented electrical steel (GOES) is employed for the stator teeth, which primarily experience axially directed flux in the YASA topology. GOES has a higher permeability and lower losses than non-oriented electrical steel for flux in the direction of the grain [10], [11]. Thus, YASA motors with GOES stators can achieve improved efficiencies [10]. The rotor magnets are arranged in a Halbach array to provide a more sinusoidal flux distribution, which can

TABLE I. ASCEND Program System Targets [3]

Takeoff mechanical shaft power output	≥ 250 kW
Maximum rotational speed at takeoff	5,000 RPM
Specific power at takeoff	≥ 12 kW/kg
Takeoff and climb average efficiency	≥ 93%
Cruise mechanical shaft power output	≥ 83 kW
Cruise rotational speed	3,500 RPM – 4,500 RPM
Average cruise efficiency	≥ 93%

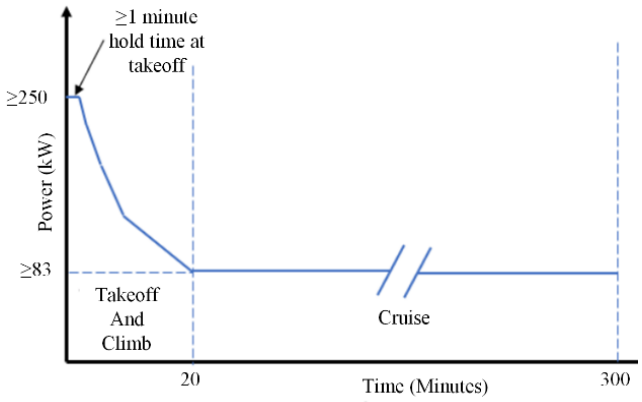

Fig. 1. ARPA-E ASCEND flight profile requirement for mechanical power as a function of time [3].

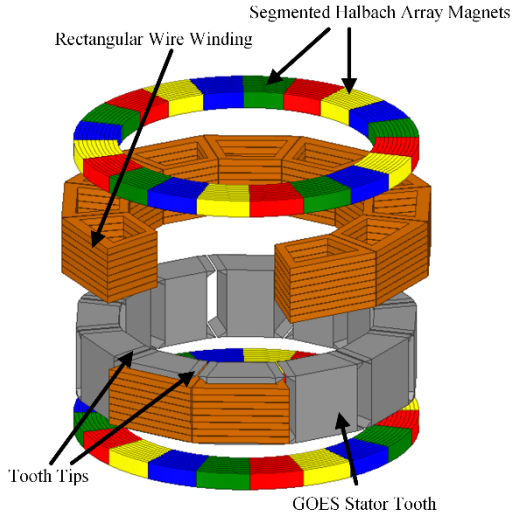

Fig. 2. Exploded view of the motor topology with 12 slots and 5 pole pairs.

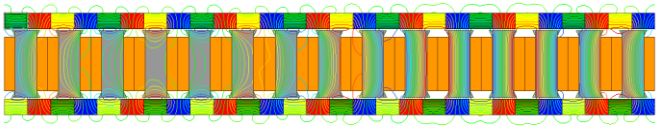

Fig. 3. 2D flux lines distribution of a symmetrical fraction of an example "unrolled" motor design with 30 slots and 14 pole pairs.

reduce core losses and cogging torque [12]. Additionally, the Halbach array provides a return path for magnet flux [13], allowing the rotor back irons to be replaced with a lightweight carbon fiber reinforced polymer. Fig. 3, which illustrates the flux paths in an "unrolled" 2D model of an example design, demonstrates the significantly reduced leakage flux axially beyond the motor. The permanent magnets are segmented to reduce eddy current losses [14]. Tooth tips also reduce eddy current losses in the magnets and windings and smooth the airgap surface, which results a more sinusoidal airgap flux density. Wires with rectangular cross-sections provide a higher copper fill factor than conventional round wires, which can increase power densities and reduce losses [15], [16]. Furthermore, the YASA topology has two air-gaps, which reduces the stator inductances relative to other topologies and can improve the power factor (PF) [17].

Since there is no control over PM excitation, interturn short circuit (ITSC) faults are a high-risk phenomenon in PM machines. Ref. [18] shows that the typical method of shorting the phase terminals may not adequately alleviate the ITSC fault current in form-wound machines. Multiple mitigation techniques, including phase terminal shorting, current injection, vertical windings, electrical and mechanical shunts were compared in [19] and [20]. Redundancy is another common approach to achieve fault tolerance. For example, [21] proposes a dual winding arrangement to have a six phase PM machine. In case of an ITSC fault, the remaining healthy phases drive the motor, making up for the power of the faulted phases, so the system can continue normal operation. Refs. [22]-[24] discussed the tradeoffs for different fault tolerant methods in terms of weight, cost, complexity, and reliability. All the methods above come with some disadvantages. For example, current injection can effectively reduce the ITSC fault current, but it increases the copper loss and derates the machine. Shunting techniques add extra weight and cost to the system. Redundancy requires significant overdesign. Additionally, the above methods rely on the ability to detect ITSC faults, which is challenging [25]. Therefore, in this paper a new winding arrangement based on form wound coils is used that can inherently block or reduce ITSC fault currents and simplifies detection of ITSC faults [26].

The first step in the co-design process is to characterize each of the subsystems throughout the design space so that a design can be selected for optimal system-level performance. Thus, rather than simply optimizing the motor design, this paper focuses on characterizing the motor's electromagnetic performance, identifying tradeoffs that will affect both the motor and another subsystem (eg. drive or TMS), and quantifying the impacts of these tradeoffs on motor performance. For example, the number of poles affects the electromagnetic performance of the motor and the fundamental frequency of the drive. As another example, the inner and outer surface area of the end windings is the primary area through which the TMS must remove heat from the motor and depends on motor design parameters, such as the stator axial length and the outer radius. (The TMS includes a pumped cooling system where the ethylene-glycol/water mixture used as a coolant transfers heat from microchannel heatsinks installed on the stator's outer end windings to air heat exchangers. Additionally, zeolite adsorbents placed on the inner end windings dissipate the extra heat generated during take-off.) This approach, when coupled with similar characterizations of the other subsystems, provides a flexible optimization process for determining the system-level optimal design, even when faced with evolving constraints and objectives. Additionally, this paper evaluates many different slot/pole combinations while allowing the geometry to vary, in order to characterize their achievable performances. Then, in this paper, as a continuation of [27], a design is selected for further evaluation of PF and AC losses in the PMs and windings with different number of PM pieces and different winding temperatures.

Thus, the contributions of this paper include the following:

- Evaluation of a high performance YASA motor integrating GOES stator teeth, rectangular wire winding, and rotors with Halbach arrays and nonmagnetic cores
- 3D finite element analysis (FEA) comparison of 12 different slot/pole combinations for a YASA motor

- Characterization of the motor's electromagnetic performance in terms of its interfacial parameters with the other subsystems
- An innovative six-phase winding arrangement for mitigating interturn short-circuit fault currents

II. Design Study Methodology

Fig. 4 shows a prototype conical air gap YASA motor, for which the 3D FEA models were previously validated against experimental results [10]. While the current study considers a flat air gap YASA motor, the results from [10] are used to validate the core loss model for the GOES stator teeth. Note that the stator teeth in the flat air gap motor are simpler than in the conical air gap motor; thus, if the 3D FEA could accurately predict the core losses in the more complex stator teeth, it should be able to accurately predict the core losses in the stator teeth of the current study. (The Fig. 4 motor also provides proof of manufacturability for the stator teeth.) Moreover, FEA is known for its high accuracy in torque prediction [28], as in [10]. Thus, 3D FEA was employed to analyze a wide range of designs for this study.

In general, the FSCW configuration has the advantages of a high slot fill factor and short end windings, but it tends to produce additional spatial harmonics, which can result in significant rotor PM losses [29]. Therefore, there have been studies on pole counts and stator slot counts to find the optimal combinations for key performance indices, such as fundamental winding factor and periodicity, which were verified by FEA for radial flux machines [30], [31]. In an AFPM motor, the presence of symmetry (periodicity > 1) cancels out the off-axis torques on the rotor to prevent significant noise and vibration [32]. Table II lists several viable, high-performance slot/pole pair (PP) combinations for tooth-wound motors. In this paper, designs with these different slot/PP combinations are evaluated using 3D FEA.

However, unlike previous studies [30], [31], the machine's geometric parameters, whose values are presented in Table III, are also swept for each slot/PP combination to better compare the achievable performance with each slot/PP combination, as the optimal geometric parameters may depend on the slot/PP combination. Magnetostatic simulations with fixed RMS current densities (29.7 A/mm^2 and 35.6 A/mm^2) were used for the initial analysis to assess which designs might achieve the peak takeoff requirements. These high current densities will only be applied during the limited takeoff time shown in Fig 1. Additionally, the TMS will aggressively extract heat directly from the inner and outer surfaces of the end windings during takeoff and climb. The current density is interpolated in post-processing to produce the required peak torque of 480 Nm. The wire cross-sections and the number of turns can be selected later to determine the terminal voltages and currents

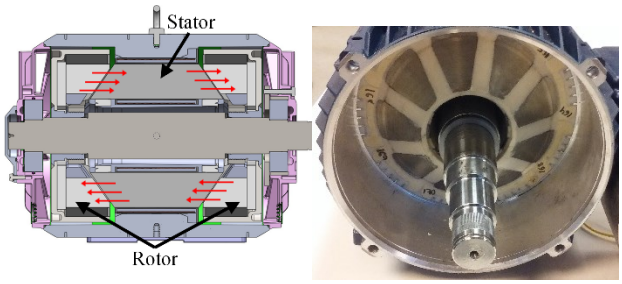

(a) (b)

Fig. 4. (a) Transverse-section (with red arrows illustrating flux direction) and (b) prototype stator of YASA motor with GOES in [10] used to validate FEA models.

TABLE II. Slot/Pole Pair Combinations

Slots/PP	Fundamental winding factor	Periodicity
12/5	0.933	2
18/8	0.945	2
24/10	0.933	4
24/11	0.949	2
24/14	0.933	4
27/12	0.945	3
30/14	0.951	2
36/16	0.945	4
36/17	0.953	2
42/20	0.953	2
45/24	0.951	3
48/26	0.9495	4

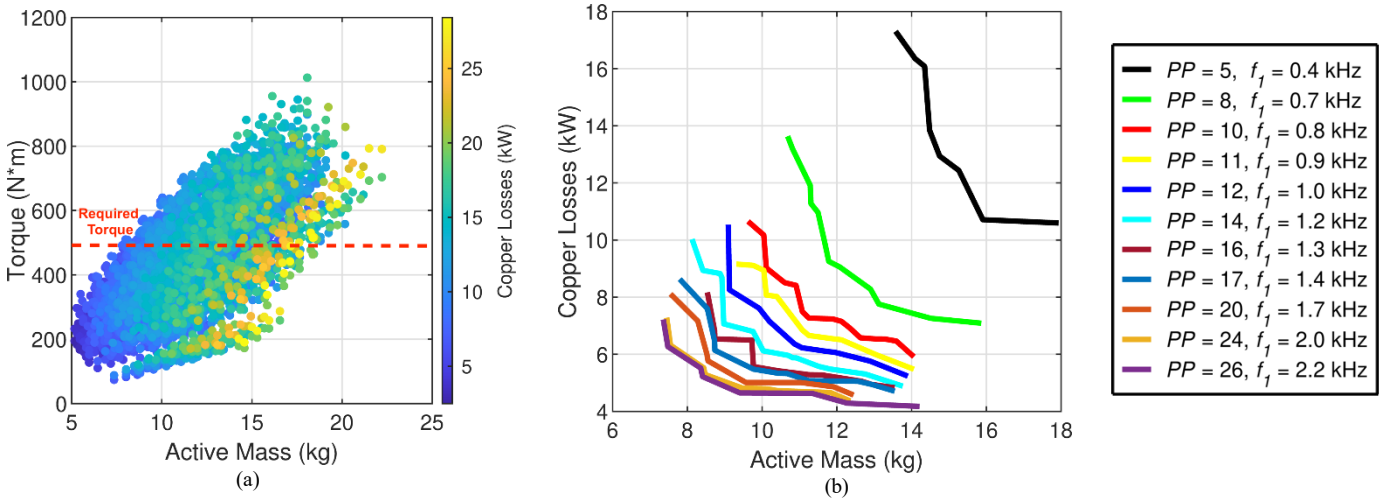

Fig 5. (a) Average torque, copper losses, and total active masses of the simulated cases and (b) Pareto fronts for minimum total active mass and minimum copper losses for different pole pair counts (and, thus, different fundamental frequencies). Only designs with at least 480 Nm of torque are included in Fig. 5(b).

TABLE III. PARAMETERS FOR INITIAL MAGNETOSTATIC SIMULATIONS

Name	Description	Values	Units
R_{2S}	Stator Teeth Outer Radius	120,135	mm
R_{1S}	Stator Teeth Inner Radius		
	For R_{2S} = 120	80,85,90,95	mm
	For R_{2S} = 135	100,105,110,115	mm
L_S	Stator Teeth Axial Length		
	For R_{2S} = 120	35,40,45,50	mm
	For R_{2S} = 135	25,30,35,40	mm
FF_{Cu}	Copper Fill Factor	0.8	
k_{tw}	Tooth Width to Tooth Pitch Ratio	0.4,0.5,0.6	
J	RMS Current Density	29.7, 35.6	A/mm^2
A_g	Airgap Thickness	1	mm
L_{Rotor}	Magnet Axial Thickness	5,10,15,20	mm
ω_t	Takeoff Speed	5000	RPM
ω_c	Cruise Speed	4000	RPM

to meet the requirements of the drive. Based on the simulation results, the highest performing designs were selected, and these designs were evaluated using a transient FEA model to determine core losses and power factor.

III. SIMULATION RESULT

Fig. 5(a) shows the raw (before current density interpolation) magnetostatics simulation results and which cases exceed the required 480 Nm takeoff torque. Fig. 5(b) shows the Pareto front of each PP case for minimizing the total active mass and copper losses based on the Table III design parameters. Fig. 5(b) only includes points which produce at least 480 Nm. The overall trend indicates that lower active masses and copper losses are achievable by increasing PP, if the other geometric parameters are allowed to vary.

Fig. 6 shows the achievable active mass torque densities for different rotor magnet axial thicknesses and PP values. Since the Halbach array provides the flux return path (instead of the rotor back iron), designs with fewer PP require thicker magnets, which increases the active mass. Thus, even though there is not a large difference in the fundamental winding factors in Table II, the designs with more poles are able to achieve higher torque densities. However, increasing PP beyond 24 does not provide a significant improvement due to high leakage flux through the much shorter paths between adjacent poles. Moreover, increasing PP requires a higher fundamental frequency (f_1) from the drive design perspective and can increase the core losses. Additionally, increasing PP and slot counts increases the number of magnet pieces and teeth that are needed for assembling the motor, increasing assembly complexity and the complexity of the TMS.

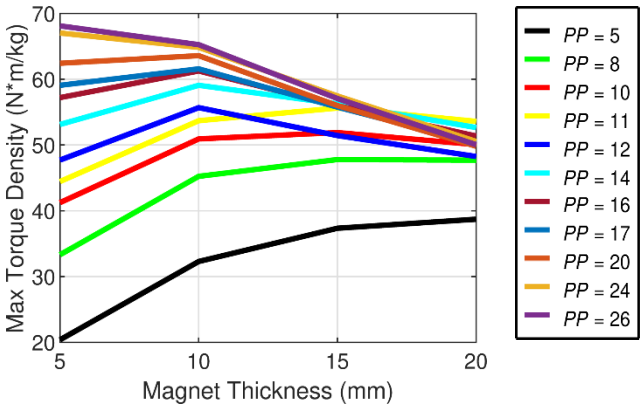

Fig 6. Maximum torque density with different magnet thickness and PP values.

Fig. 7 shows that the designs with a 135 mm stator teeth outer radius can achieve much better performances than the designs with 120 mm stator teeth outer radius. The larger outer radius yields a larger torque arm, which allows the same torque to be produced with less tangential force. Based on these results, designs with a 150 mm stator teeth outer radius were added to the study. However, only slot/PP combinations of 36/17 and 42/20 were evaluated for the 150 mm stator teeth outer radius, as these combinations represent a compromise between improved performance and avoiding excessive complexity. Table IV summarizes these additional designs.

Fig. 8 shows all the designs that achieved the 480 Nm takeoff requirement with less than 10 kW of copper losses and9 kg of active mass. These designs were evaluated with transient models for takeoff and cruise conditions. For the takeoff condition, the current density was determined based on the magnetostatic results. For the cruise condition, the designs were simulated at RMS current densities of 10, 15, and 20 A/mm^2, and the appropriate current density to achieve 200 Nm was interpolated.

Figs. 9(a) and (b) illustrate the efficiencies in takeoff and cruise conditions, respectively. Figs. 10(a) and (b) illustrate

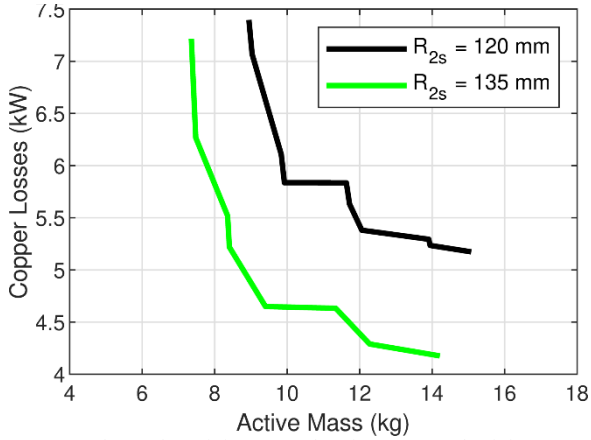

Fig 7. Pareto fronts for minimum total active mass and minimum copper losses for different stator teeth outer radii. Only designs with at least 480 Nm of torque are included.

TABLE IV. ADDITIONAL CASES AT LARGER RADIUS

Name	Description	Values	Units
R_{2S}	Stator Teeth Outer Radius	150	mm
R_{1S}	Stator Teeth Inner Radius	1250, 130, 135	mm
L_S	Stator Teeth Axial Length	20, 25, 30, 35, 40	mm
FF_{Cu}	Copper Fill Factor	0.8	
k_{tw}	Tooth Width to Tooth Pitch Ratio	0.4,0.5,0.6	
J	RMS Current Density	29.7, 35.6	A/mm^2
A_g	Airgap Thickness	1	mm
L_{Rotor}	Magnet Axial Thickness	5,10,15,20	mm

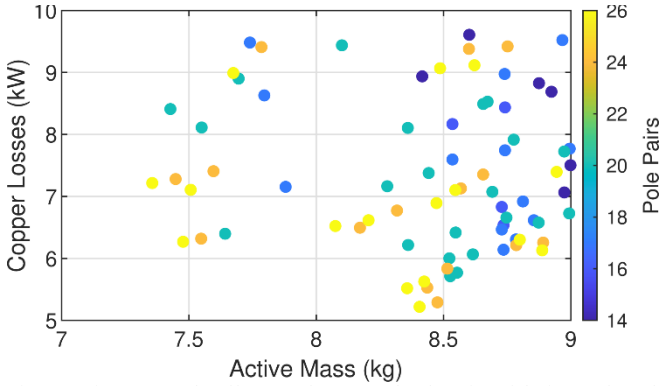

Fig 8. Active mass, takeoff copper losses, and pole pairs of designs selected for transient analysis.

what percentage of the electromagnetic losses is from copper loss for each of these designs in takeoff and cruise conditions, respectively. These calculations assume that the losses are dominated by DC copper losses and core losses in the stator laminations. Mechanical losses are neglected, eddy current losses in the magnets are assumed to be small due to magnet segmentation, and AC copper losses are also assumed to be small because the tooth tips shield the windings from the rotor flux. These designs show promising efficiencies at both takeoff (480 Nm, 5000 RPM) and cruise (200 Nm, 4000 RPM) conditions. Fig. 9(a) does not show a strong correlation between PP and efficiency at takeoff; as shown in Fig. 5(b), designs with higher PP can achieve lower copper losses for a given active mass, but these designs also experience higher frequencies, leading to increased core loss densities. Thus, the designs with higher PP tend to have lower copper loss

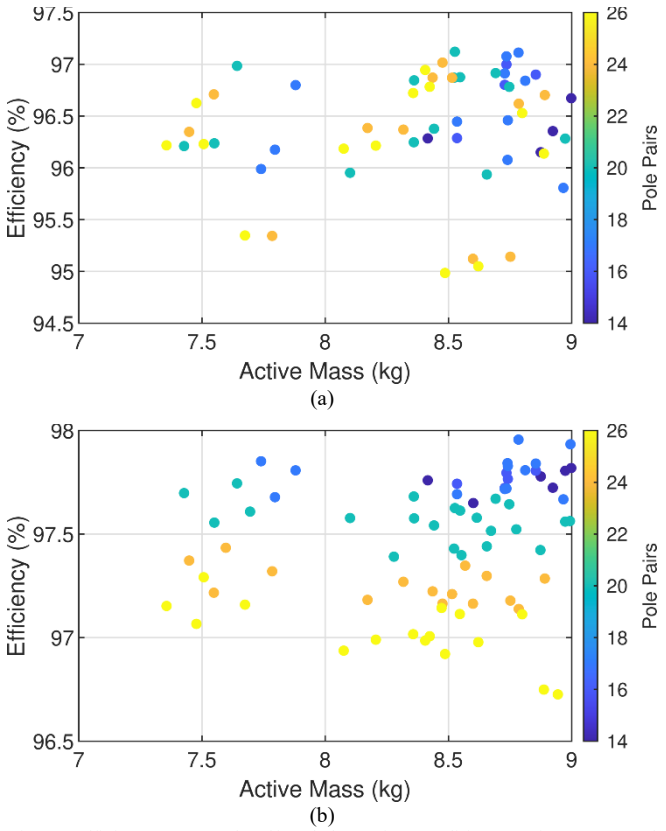

Fig. 9. Efficiency at (a) takeoff and (b) cruise conditions, active mass, and pole pairs.

percentages in Fig. 10(a). Fig. 9(b) generally shows higher cruise efficiencies than takeoff efficiencies because the copper losses are dominant at takeoff but decrease quadratically with current density. Additionally, Fig. 9(b) shows a correlation between PP and efficiency. Because the reduced torque at cruise significantly reduces copper losses, the core losses are more significant for all designs, especially those with higher PP, as illustrated in Fig. 10(b).

Fig. 11 illustrates various tradeoffs between active mass, takeoff efficiency, design parameters, and parameters that affect other subsystems (eg. end winding outer surface area). Fig. 11(a) illustrates the tradeoffs between minimizing the active mass, maximizing the efficiency, and maximizing the outer surface area of the end windings. The designs with the lowest masses and highest efficiencies tend to have less end winding surface area. However, the designs with higher efficiency may require less end winding surface area because the TMS will not need to remove as much heat. Fig. 11(b) shows the axial force on the rotors of each design at the takeoff condition. The larger the axial forces, the heavier the rotor support system will need to be, increasing the total (active plus inactive structural) mass of the motor. Fig. 11(c) shows the current densities of each of the designs at the takeoff condition. The designs with the very smallest active masses tend to have current densities near the upper limit so that they can produce the most torque with the least active material. However, the designs with the very highest efficiencies tend to have lower current densities because the copper loss density scales with the square of the current density.

Figs. 11(d)-(h) show various geometric parameters, and Fig. 11(i) shows the surface area of an airgap for each of the

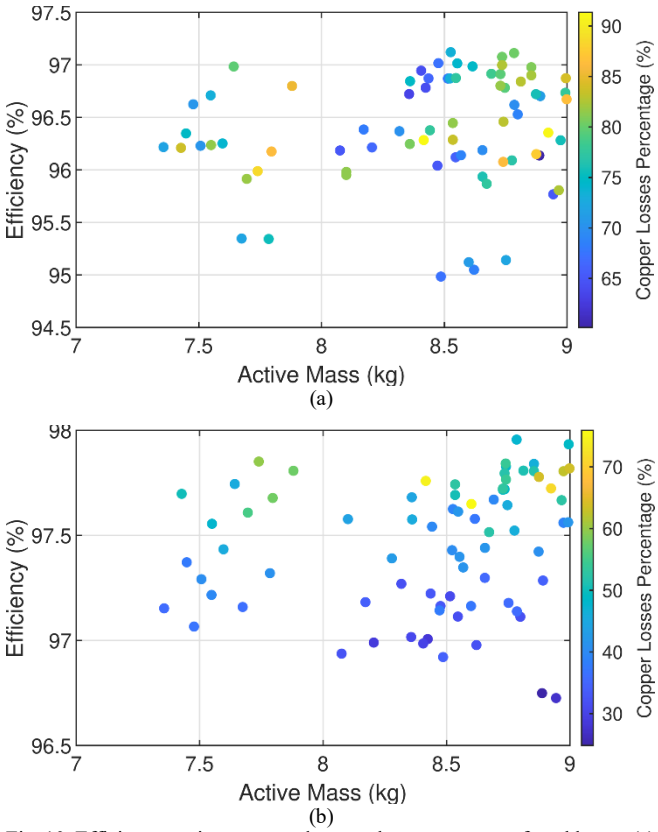

Fig. 10. Efficiency, active mass, and copper loss percentage of total loss at (a) takeoff and (b) cruise conditions.

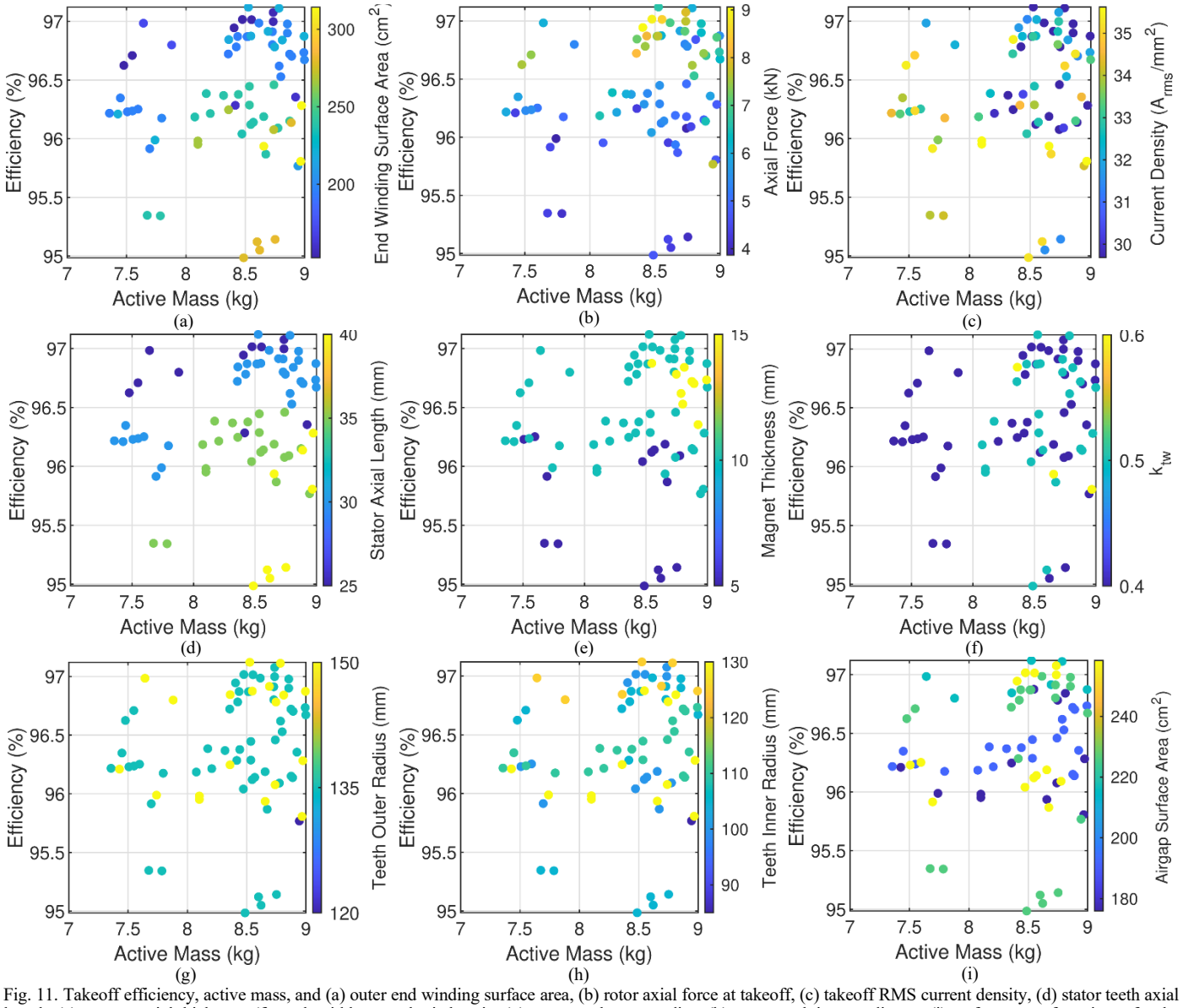

Fig. 11. Takeoff efficiency, active mass, and (a) outer end winding surface area, (b) rotor axial force at takeoff, (c) takeoff RMS current density, (d) stator teeth axial length, (e) magnet axial thickness, (f) tooth width to tooth pitch ratio, (g) stator teeth outer radius, (h) stator teeth inner radius, or (i) surface area of an airgap for the designs evaluated with transient simulations.

designs. The axial forces are strongly correlated with the magnet thicknesses and airgap surface areas; increasing either the magnet thickness or the air gap surface area tends to increase the axial forces on the rotors. Fig. 11(d) shows that the 25 mm and 30 mm stator axial length designs are electromagnetically optimal; the designs with larger stator axial lengths tend to be heavier and less efficient. On the other hand, none of the designs with a 150 mm stator teeth outer radius and 20 mm stator axial length achieved the target torque with acceptable mass and losses. However, increasing the stator length increases the end winding surface area, which can facilitate better cooling. Additionally, the designs with longer stator lengths tend to have thinner magnets or reduced airgap surface areas, decreasing the axial forces on the rotors. Fig. 11(e) shows that the optimal magnet thickness is near 10 mm. The designs with 15 mm or 20 mm thick magnets are too heavy, whereas the designs with 5 mm thick magnets tend to be less efficient because more amp-turns are required to produce the necessary torque. Fig. 11(f) shows that the optimal designs have a tooth width to tooth pitch ratio of 0.4, meaning that the stator slots are tangentially wider than the stator teeth. Increasing k_{tw} increases the surface area of the tooth, potentially allowing more flux to pass through the stator. However, increasing k_{tw} also reduces the slot width and requires an increase in stator length, airgap surface area, or current density to achieve the required torque. Increasing stator length or airgap surface area increases the active mass, whereas increasing current density increases the copper loss density. Fig. 11(g) shows that the smallest outer radius considered did not yield adequate performance. Increasing the stator teeth outer radius to 150 mm allows the radial thickness or axial length of the stator teeth to decrease, but this does not reduce the active mass as much as going from 120 mm to 135 mm for the stator teeth outer radius. However, the larger outer radius for the stator teeth results in a larger outer radius for the magnets, which increase the rotor support structure mass.

Figs. 12(a) and (b) present the approximate PF in takeoff and cruise conditions, respectively. In this calculation, the PF is estimated for max torque per amp (MTPA) operation from

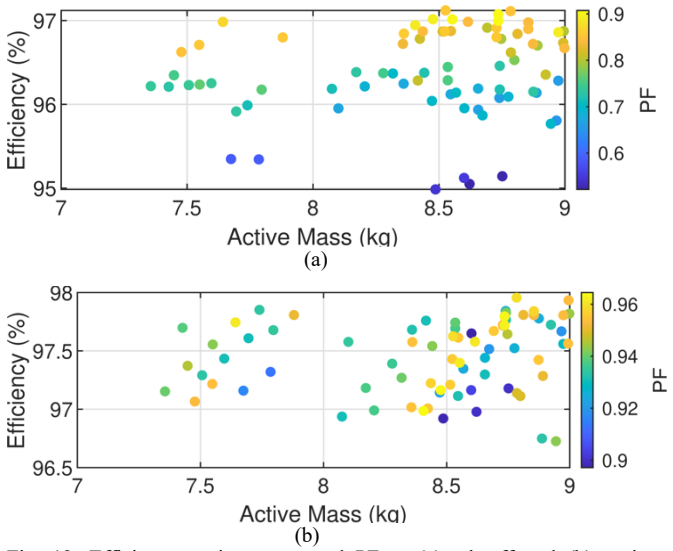

Fig. 12. Efficiency, active mass, and PF at (a) takeoff and (b) cruise conditions for MTPA operation.

the back emf coefficient and the apparent inductances. Fig. 12(a) shows that the designs with higher takeoff efficiencies tend to have higher PF. The designs with lower efficiencies will tend to have higher copper losses, correlating to having more amp-turns, or higher core losses, due to higher fundamental frequencies or higher stator teeth volumes. Increasing the stator teeth volume will tend to increase the inductances. Thus, the designs with lower takeoff efficiencies tend to have more reactive power at takeoff. However, Fig. 12(b) shows that when the currents are significantly decreased in cruise mode, all the designs have high PF in MTPA operation, due to the relatively low inductance of the YASA topology [17].

While the previous results assume a magnet temperature of 100 °C, more aggressive cooling could potentially keep the magnets at a lower temperature. Thus, similar magnetostatic simulations were run for magnet temperatures of 80 °C. Fig. 13 compares the Pareto fronts for the simulations at the two temperatures for some pole pair counts. Fig. 13 shows a relatively minor reduction in active mass and copper losses. However, a slightly more significant improvement might be achieved if the reduced temperature allowed a higher magnet grade to be used without being demagnetized.

IV. Optimum Design Parameters

The stated studies up to this point of the paper evaluate the set of selected designs that match the demanding torque, efficiency, etc. However, based on the demands of other subsystems and the limited potential improvements, additional constraints are applied. The PP count is limited to 20 due to manufacturing complexity, especially for the TMS. The rotor outer radius is capped at 135 mm to avoid increasing structural mass. Hence, Table V shows the key parameters of a design selected for further analyses.

Here, the PF is evaluated based on the simulated induced voltage on the coils. Table VI shows the effects of changing the current angle relative to the back-emf on PF and rotor torque at takeoff condition where each case has the same

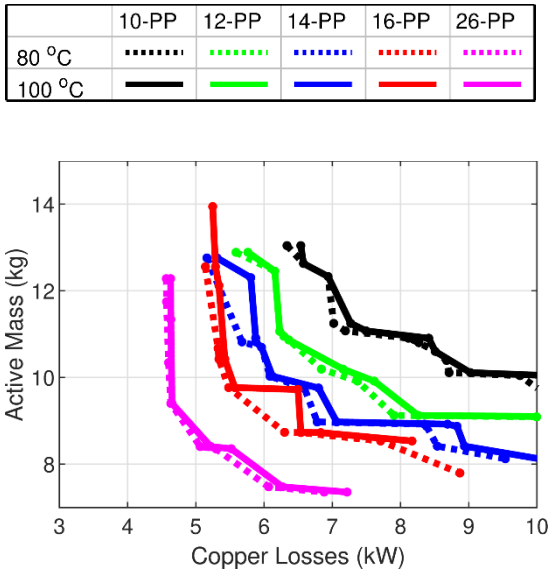

Fig. 13. Pareto optimal fronts for minimizing active mass and copper losses for different pole counts assuming 80 °C or 100 °C magnet temperature.

TABLE V. Selected Design Key Parameters

Name	Description	Values	Units
R_{2S}	Stator Teeth Outer Radius	135	mm
R_{1S}	Stator Teeth Inner Radius	110	mm
L_S	Stator Teeth Axial Length	30	mm
T_{coil}	Coil Thickness	4.2	mm
J	RMS Current Density	35.6	A/mm^2
A_g	Airgap Thickness	1	mm
L_{Rotor}	Magnet Axial Thickness	10	mm
	Number of Teeth	42	
PP	Pole pairs	20	
	RMS Back EMF	363	V

TABLE VI. Impacts of Current Angle at Takeoff Condition

Current Angle (deg)	Torque (Nm)	PF	Number of Turns per Tooth
0	486	0.82	16
5	494	0.84	16
10	499	0.86	18
15	497	0.87	18
20	490	0.89	18
25	479	0.90	20

number of Ampere-turns in each slot. The number of turns was determined to keep the line-to-line motor voltages at takeoff appropriate for an inverter with a 1 kV DC bus. A 20deg current angle is selected to increase the PF to 0.89. Furthermore, due to the significant saturation of the stator teeth, the torque slightly increased to 490 Nm in field weakening mode.

To improve reliability, a new winding arrangement (Fig. 14) that can block or reduce ITSC fault currents in machines with form-wound winding is used [26]. The winding arrangement includes two sets of three phase windings that are in phase and do not share a neutral point. The conductors are arranged such that no conductor is adjacent to another conductor of the same phase or a phase that shares a common neutral point. In this arrangement, any faults between turns become phase-phase faults, which must pass through the

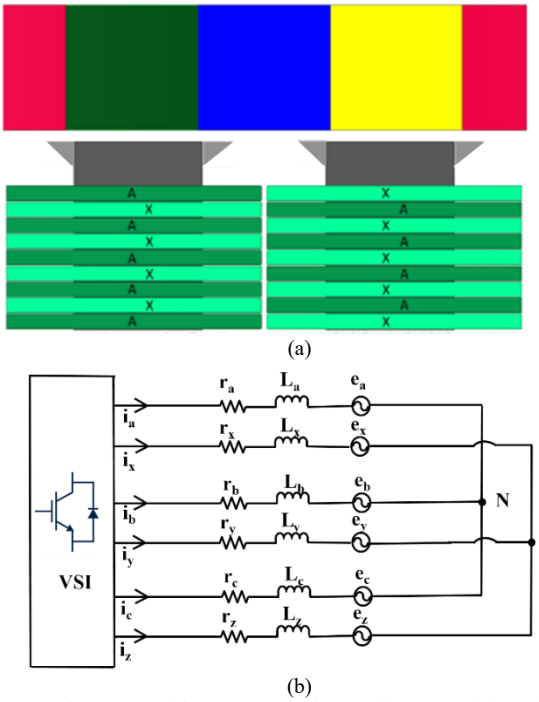

(a)

(b)

Fig. 14. (a) Placement of the turns around two adjacent teeth based on the proposed winding arrangement. (b) Equivalent circuit of the machine with the six-phase voltage source inverter (VSI) during healthy operation [26]

inverter, where the current can be blocked. Alternatively, the voltages supplied to the windings can be modified, and the fault current can potentially be reduced to an acceptable level, allowing the machine to continue functioning close to normal operation [26]. Finally, this arrangement simplifies winding short-circuit fault detection, as the fault current is simply the sum of the phase currents in any three-phase set. The characteristic current of the model is 130 A_{rms}, which is less than the 152 A_{rms} phase currents at takeoff. Therefore, inverter short-circuit faults can still be mitigated by shorting the phase terminals.

V. Detailed Electromagnetic Loss Investigation

The DC copper losses and core losses are the major electromagnetic loss sources of the powertrain. However, for accuracy in the design study, the AC losses in the windings and magnet losses should also be evaluated [33].

The magnet material is assumed to be NdFeB N48SH at 100 °C temperature. The magnets' proximity to the teeth causes them to experience eddy current losses. At the 250 kW operating point, the FEA predicts 1.56 kW of magnet eddy current losses. In order to reduce this loss, the magnets were segmented in the radial direction, as shown in Fig. 15(a).

The number of segments was parameterized to study the effect on the losses and torque. Fig. 15(b) shows the impacts of the number of segments on magnet eddy current losses and torque for a fixed number of Ampere-turns in each slot. Increasing the number of segments reduces losses, but this also reduces the torque due to the reduced magnet volume. Therefore, the number of segments is selected to be 9.

Previously, only the DC portion of the copper losses was considered; however, there are also AC effects, such as skin depth and eddy currents in the windings. To evaluate these

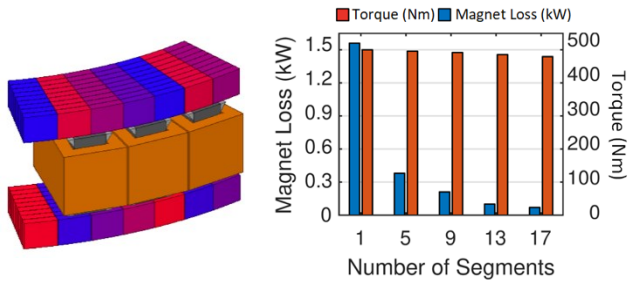

Fig. 15 (a) Fig. 15(b)

Fig. 15. (a) Segmented magnets in both the rotors (b) Impact of segments on magnet loss and motor torque at takeoff condition

losses, each coil is divided into individual turns for the FEA simulations. Additionally, the windings were simulated at different temperatures to help determine the target winding temperatures that would optimize system-level performance. Table VII shows the total AC and DC winding losses at 3 different temperatures. In this case, the temperature has a surprisingly small impact on total winding losses because increasing the temperature significantly reduces AC losses.

Based on the thorough loss studies, Table VIII provides the predictions of the total motor electromagnetic losses at the takeoff and cruise operating points if the windings are at 150 °C. A margin of error for FEA imprecision and tolerances in the manufacturing is included. Considering the margin of error, the proposed model marginally obtains the target takeoff and climb efficiency.

VI. Summary of Results

- The current density contributes to the tradeoff between active mass and efficiency. The minimum active mass designs tend to have higher current densities, whereas the maximum efficiency designs tend to have lower current densities.
- While a large number of pole pairs increases the fundamental frequency that the drive must supply, it can reduce the active mass and copper losses of the motor for a certain specs requirement. One reason that this occurs is that lower pole counts require thicker magnets in the Halbach array for the flux return path in the rotor. However, increasing the number of pole pairs increases the motor and TMS complexity. Additionally, increasing the number of pole pairs increases the core losses; thus, designs with higher pole counts achieved comparable

TABLE VII. Winding Losses at Difrent Winding Temperatures at Takeoff and Cruise Operation Points

Output Power (kW)	Winding Loss at 90 °C (kW)		Winding Loss at 120 °C (kW)		Winding Loss at 150 °C (kW)	
	DC Loss	AC Loss	DC Loss	AC Loss	DC Loss	AC Loss
250	7.63	3.71	8.31	3.32	9.00	2.95
83	0.77	1.81	0.84	1.75	0.91	1.67

TABLE VIII. Total Electromagnetic Loss and Efficiency at Takeoff and Cruise Operating Points with 150 °C Winding Temperature

Output Power (kW)	Winding Loss (kW)	Core Loss (kW)	Magnet Loss (kW)	Margin (kW)	Efficiency (%)
250	11.95	2.21	0.21	1.00	93.85
83	2.59	1.32	0.08	0.33	94.36

takeoff efficiencies to designs with lower pole counts. However, during cruise conditions, the designs with higher pole counts achieved lower efficiencies because the core losses contributed a larger percentage of the electromagnetic losses than during takeoff.

- The outer radius provides another tradeoff. Increasing the outer radius can improve electromagnetic performance, but it will also increase the amount of material required to mechanically support the rotor.
- The axial forces on the rotors are largely driven by the magnet thickness and the airgap surface area. Thus, designs with larger stator teeth lengths and reduced airgap surface areas or reduced magnet thicknesses can require less rotor support material. Additionally, increasing the stator teeth length tends to increase the end winding surface area, which can facilitate better heat extraction from the windings.
- There is a tradeoff between segmenting magnet pieces to reduce the induced eddy current losses, the torque reduction due to the magnet volume reduction, and the increased fabrication complexity.
- The PF analysis shows that, in addition to improving PF, a small field weakening angle can increase the torque, due to heavy saturation of the stator teeth.
- In the winding losses investigation, although the DC copper losses rise significantly at higher temperature, the reduction in AC copper losses resulted in a relatively small change in total copper losses as temperature varied.

VII. Conclusion

This paper evaluates a YASA motor with segmented Halbach array magnets, rectangular wires, and grain oriented electrical steel for a 250 kW electric aircraft propulsion application. The 3D FEA results show that the motor can achieve the necessary torque for takeoff with less than 8 kg of active mass and electromagnetic efficiencies around 94%.

This paper provides an extensive 3D FEA comparison of different slot/pole combinations for a YASA motor with Halbach array magnets.

This paper also presents an innovative six-phase winding arrangement to mitigate interturn short-circuit fault currents.

Because the electric aircraft requires the mass and efficiency of the entire drivetrain to be optimized, the motor must be tightly integrated and co-designed with the thermal management system, inverter, and structural design. Thus, rather than merely optimizing the electromagnetic performance of the motor or even employing a multiphysics optimization, the motor's electromagnetic performance is characterized in terms of the parameters at the interfaces with the other subsystems. This includes characterizing the impact of design variables on parameters that affect the other subsystems, such as the axial forces on the rotor and the heat generated by losses, and evaluating the impacts of other interfacial parameters, such as winding and magnet temperatures, on the electromagnetic behavior. In future work, this characterization will be coupled with similar characterizations of the other subsystems to determine the system-level optimal design. This approach provides more flexibility to adapt to evolving constraints and objectives than a traditional optimization algorithm, such as a genetic algorithm.

Generally, the magnetic performance can be improved by using a high number of pole pairs, a large outer radius, and short stator teeth. However, such a design does not necessarily yield the optimal system-level performance. Reducing the number of pole pairs can reduce complexity and improve cruise efficiency. Using longer stator teeth with a smaller airgap surface area can increase the end winding surface area, facilitating better cooling, and reduce the axial forces on the rotors, reducing the required structural mass.

Acknowledgment

Portions of this research were conducted with the advanced computing resources provided by Texas A&M High Performance Research Computing. The authors would like to thank ANSYS for their support of the EMPE lab through the provision of FEA software.

This material is based upon work supported by the Department of Energy under Award Number DE-AR0001356. This report was prepared as an account of work sponsored by an agency of the United States Government. Neither the United States Government nor any agency thereof, nor any of their employees, makes any warranty, express or implied, or assumes any legal liability or responsibility for the accuracy, completeness, or usefulness of any information, apparatus, product, or process disclosed, or represents that its use would not infringe privately owned rights. Reference herein to any specific commercial product, process, or service by trade name, trademark, manufacturer, or otherwise does not necessarily constitute or imply its endorsement, recommendation, or favoring by the United States Government or any agency thereof. The views and opinions of authors expressed herein do not necessarily state or reflect those of the United States Government or any agency thereof.

References

[1] B. Sarlioglu and C. T. Morris, "More electric aircraft: review, challenges, and opportunities for commercial transport aircraft" *IEEE Trans. Transport. Electrific*., vol. 1, no. 1, pp. 54-64, Jun. 2015.

[2] F. Kelch, Y. Yang, B. Bilgin, and A. Emadi, "Investigation and design of an axial flux permanent magnet machine for a commercial midsize aircraft electric taxiing system," *IET Electr. Syst. Transp*., vol. 8, no. 1, pp. 52-60, Mar. 2018.

[3] "DE-FOA-0002238: Aviation-class synergistically cooled electric-motors with integrated drives (ASCEND)", Department of Energy, Advanced Research Projects Agency Energy, Dec. 16, 2019.

[4] "Siemens develops world-record electric motor for aircraft," Siemans, Mar 2015, Press. [Online]. Available: https://press.siemens.com/global/en/pressrelease/siemens-develops-world-record-electric-motor-aircraft.

[5] N. Taran, G. Heins, V. Rallabandi, D. Patterson, and D. M. Ionel, "Evaluating the effects of electric and magnetic loading on the performance of single- and double-Rotor axial-flux PM machines," *IEEE Trans. Ind. Appl*, vol. 56, no. 4, pp. 3488-3497, Jul.-Aug. 2020.

[6] B. Zhang, Y. Wang, M. Doppelbauer and M. Gregor, "Mechanical construction and analysis of an axial flux segmented armature torus machine," in *Proc. IEEE Int. Conf. Elect. Mach.*, 2014, pp. 1293-1299,

[7] P. Ojaghlu and A. Vahedi, "A New Axial Flux Permanent Magnet Machine," *IEEE Trans. Magn*., vol. 54, no. 1, pp. 1-6, Jan. 2018

[8] N. Taran, G. Heins, V. Rallabandi, D. Patterson, and D. M. Ionel, "Systematic comparison of two axial flux pm machine topologies: Yokeless and segmented armature versus single sided", in *Proc. IEEE Energy Convers. Congr. Expo*, 2019, pp. 4477-4482.

[9] T.J. Woolmer, M.D. McCulloch, " Analysis of the yokeless and segmented armature machine", in *Proc. IEEE Int. Elect. Mach. Drives Conf.*, 2007, pp. 704-708.

[10] M. C. Gardner, Y. Zhang, D. Talebi, H. A. Toliyat, A. Crapo, P. Knauer, and H. Willis, "Loss Breakdown of a Dual Conical Rotor Permanent Magnet Motor using Grain Oriented Electrical Steel and Soft Magnetic Composites", in *Proc. IEEE Int. Elect. Mach. and Drives Conf*., 2019, pp. 1067-1074.

[11] D. Kowal, P. Sergeant, L. Dupr, and A. Van den Bossche, "Comparison of nonoriented and grain-oriented material in an axial flux permanent-magnet machine", *IEEE Trans. Magn*., vol. 46, no. 2, pp. 279-285, Feb. 2010.

[12] Z. Q. Zhu and D. Howe, "Halbach permanent magnet machines and applications: A review", *IEE Proc.-Elect. Power Appl*., vol. 148, no. 4, pp. 299-308, Jul. 2001.

[13] M. Johnson, M. C. Gardner, and H. Toliyat, "Analysis of axial field magnetic gears with Halbach arrays", in *Proc. IEEE Int. Elect. Mach. Drives Conf*., 2015, pp. 108-114.

[14] P. Sergeant and A. van den Bossche, "Segmentation of Magnets to Reduce Losses in Permanent-Magnet Synchronous Machines", *IEEE Trans. Magn*, vol. 44 no. 11, pp. 4409-4412, Nov. 2008.

[15] Y. Zhao, D. Li, T. Pei, and R. Qu, "Overview of the Rectangular Wire Windings AC Electrical Machine", *CES Trans. Elect. Mach Syst*, vol. 3, no. 2, pp. 160-169, Jun. 2019.

[16] J. H. Choi., Y. D. Chun, P. W. Han, M. J. Kim, D. H. Koo, J. Lee, and J. S. Chun, "Design of high power permanent magnet motor with segment rectangular copper wire and closed slot opening on electric vehicles", *IEEE Trans. Magn.*, vol. 46, no. 6, pp. 2070-2073, Jun. 2010.

[17] D. Winterborne, N. Stannard, L. Sjöberg and G. Atkinson, "An Air-Cooled YASA Motor for in-Wheel Electric Vehicle Applications," *IEEE Trans. Ind. Appl.*, vol. 56, no. 6, pp. 6448-6455, Nov.-Dec. 2020.

[18] A. J. Mitcham, G. Antonopoulos, and J. J. A. Cullen, "Implications of shorted turn faults in bar wound PM machines," *Proc. Inst. Elect. Eng.—Elect. Power Appl.*, vol. 151, no. 6, pp. 651–657, Nov. 2004.

[19] P. Arumugam, C. Gerada, T. Hamiti, C. Hill, and S. Bozhko, "A review on turn-turn short circuit fault management," in *Proc. Int. Conf. on Elect. Syst. for Aircraft, Railway, Ship Propulsion and Road Veh.*, 2015, pp. 1-5.

[20] P. Arumugam, T. Hamiti, and C. Gerada, "Modeling of Different Winding Configurations for Fault-Tolerant Permanent Magnet Machines to Restrain Interturn Short-Circuit Current," *IEEE Trans. Energy Convers.*, vol. 27, no. 2, pp. 351-361, June 2012.

[21] X. Jiang, D. Xu, L. Gu, Q. Li, B. Xu, and Y. Li, "Short-Circuit Fault-Tolerant Operation of Dual-Winding Permanent-Magnet Motor Under the Four-Quadrant Condition," *IEEE Trans. Ind. Electron.*, vol. 66, no. 9, pp. 6789-6798, Sept. 2019.

[22] A. M. El-Refaie, "Fault-tolerant permanent magnet machines," *IET Elect. Power Appl.*, vol. 5, no. 1, pp. 59–74, Jan. 2011.

[23] J. W. Bennett, G. J. Atkinson, B. C. Mecrow, and D. J. Atkinson, "Fault-Tolerant Design Considerations and Control Strategies for Aerospace Drives," *IEEE Trans. Ind. Electron.*, vol. 59, no. 5, pp. 2049-2058, May 2012.

[24] G. J. Atkinson, J. W. Bennett, B. C. Mecrow, D. J. Atkinson, A. G. Jack and V. Pickert, "Fault tolerant drives for aerospace applications," in *Proc. Int. Conf. on Integr. Power Electron. Syst.*, 2010, pp. 1-7.

[25] A. Gandhi, T. Corrigan, and L. Parsa, "Recent advances in modeling and online detection of stator interturn faults in electrical motors," *IEEE Trans. Ind. Electron.*, vol. 58, no. 5, pp. 1564–1575, May 2011.

[26] A. Daniar and M. C. Gardner, "Investigation of a Multiphase Winding Arrangement for Mitigating Short-Circuit Fault Currents", in *Proc. IEEE Int. Symp. Diagnostics for Elec. Mach. Power Electron. and Drives*, 2021, pp. 113-118.

[27] D. Talebi, M. C. Gardner, S. V. Sankarraman, A. Daniar and H. A. Toliyat, "Electromagnetic Design Characterization of a Dual Rotor Axial Flux Motor for Electric Aircraft," in *Proc. IEEE Int. Elect. Mach. and Drives Conf*., 2021, pp. 1-8.

[28] "Simulation Versus Experimental Verification [Society News]," *IEEE Ind. Appl. Magazine*, vol. 28, no. 3, pp. 88-94, May-Jun. 2022.

[29] A. M. El-Refaie, "Fractional–slot concentrated–windings synchronous permanent magnet machines: opportunities and challenges", *IEEE Trans. Ind. Electron.*, vol. 57, no. 1, pp. 107-121, Jan. 2010.

[30] P. Ponomarev, P. Lindh, and J. Pyrhönen, "Effect of Slot-and-Pole Combination on the Leakage Inductance and the Performance of Tooth-Coil Permanent-Magnet Synchronous Machines", *IEEE Trans. Ind. Electron.*, vol. 60, no. 10, pp. 4310-4317, Oct. 2013.

[31] S. Skoog and A. Acquaviva, "Pole-slot selection considerations for double layer three-phase tooth-coil wound electrical machines", in *Proc. IEEE Int. Conf. Elect. Mach.*, 2018, pp. 934-940.

[32] A. Cavagnino, M. Lazzari, F. Profumo, and A. Tenconi, "A comparison between the axial flux and the radial flux structures for PM synchronous motors", *IEEE Trans. Ind. Appl.*, vol. 38, no. 6, pp. 1517-1524, Nov.-Dec. 2002.

[33] A. Al-Qarni, A. EL-Refaie and F. Wu, "Design and Analysis of A High Specific Power Outer Rotor Surface Mounted Permanent Magnet Machine Equipped with Additively Manufactured Windings", in *Proc. IEEE Energy Convers. Congr. Expo.*, 2021, pp. 4578-4585